I-19

Formation of deuterium-carbon inventories in gaps of plasma facing components

K. Krieger[a], W. Jacob[a], D.L. Rudakov[b], R. Bastasz[c], G. Federici[d], A. Litnovsky[e], H. Maier[a], V. Rohde[a], G. Strohmayer[d], W.P. West[f], J. Whaley[c], C.P.C. Wong[f] and the ASDEX Upgrade and DIII-D teams

[a]Association EURATOM, Max-Planck-Institut für Plasmaphysik, 85748 Garching, Germany

[b]University of California-San Diego, La Jolla, CA 92093-0352, USA

[c]Sandia National Laboratories, Livermore, CA 94551-096, USA

[d]ITER Garching Joint Work Site,85748 Garching, Germany

[e]Institut für Plasmaphysik, Association EURATOM, TEC, FZ- Jülich, 52428 Jülich, Germany

[f]General Atomics, San Diego, CA 92186-5608, USA

Abstract

Plasma facing components for ITER will be manufactured as macro brush structures or with castellated surfaces. Material samples with gaps of similar geometry as intended for ITER were exposed to different plasma conditions in TEXTOR, DIII-D and ASDEX Upgrade. In all devices a decrease of both carbon and deuterium inventories at the side faces from the gap entrance into the gap with scale-lengths in the mm range is found. The fraction of D retained at the gap surfaces is in the range of 0.4-4% of the incident flux. Main parameters determining the retained D-fraction are the temperature of the respective surfaces and the carbon fraction in the incident flux. Extrapolation of tritium inventory growth rates to ITER dimensions assuming the measured retention fractions at T>200ºC and using a D/T-flux distribution with a carbon fraction of $\approx 1\%$ from B2/EIRENE simulations of an ITER H-mode discharge yields

a contribution to the increase of the total in-vessel tritium inventory in the range of 0.5-5g T/discharge.

PSI-17 keywords: Co-deposition, Deuterium inventory, Hydrocarbons, Retention, Tungsten brush

JNM keywords: C0100, H0400, P0500, R0900, T0900

PACS: 28.52.Fa, 52.25.Vy, 52.40.Hf

1. Introduction

The plasma facing armour components (PFCs) of the ITER first wall, particularly in the divertor and baffle regions, will be manufactured as macro brush structures or with castellated surfaces in order to reduce thermo mechanical stress and to minimise electromagnetic forces due to currents induced in the material. Because in the present design carbon based materials will be used for the divertor target plates, eroded carbon atoms will migrate to other locations and co-deposit with the fuel isotopes. It is not clear yet, to what extent the potentially unlimited growth of co-deposited layers and the corresponding tritium in-vessel inventory pose a problem for the operation of ITER with respect to the maximum in-vessel inventory permitted by radiation safety regulations [1]. The tritium co-deposition problem is of particular concern with respect to the possible migration of material into gaps of macro brush structures or gaps between tiles where it can redeposit at side faces hidden from direct access. For the presently known cleaning methods [2-4] only data for flat surfaces are available and it is not known yet if they will also allow to efficiently remove hydrocarbon layers from hidden areas. Therefore, the assessment of the formation of T-inventories at such areas is one of the most critical issues for the current ITER design and consequently has become a high priority item on the agenda of the International Tokamak Physics Activity (ITPA).

The main parameters determining the formation of D/T inventories at side faces of PFC gaps are the total surface area of the side faces and the growth rate of hydrocarbon layers as a function of gap geometry, local plasma properties, material temperature and sticking properties. The flux distribution of fuel and carbon impurity ions to the PFCs is determined by plasma transport processes and the carbon source distribution. Their prediction is a separate task beyond the scope of this paper. For projections to ITER, results from predictive B2/EIRENE plasma simulations [5] will be used.

Growth rates of hydrocarbon inventories at PFC side faces have been studied so far mainly by analysis of samples, which were exposed during an entire experimental campaign [6-8] and therefore provide only limited information on the influence of the different physics parameters. New experiments in TEXTOR, DIII-D and ASDEX Upgrade overcome this limitation by exposure of samples in dedicated plasma discharges using manipulator systems. This allowed for the first time the measurement of hydrocarbon layer growth rates under well-known local conditions. In ASDEX Upgrade samples were exposed in H-mode discharges both at the outer midplane plasma periphery and the outer divertor strike point zone to compare gap deposition rates at different incident flux. In DIII-D a heatable sample was exposed to a detached divertor plasma to study the dependence of the gap deposition as function of material temperature. The derived growth rates together with results from the similar experiments in TEXTOR [9,10] can be finally used to obtain an estimate for the growth rate of the ITER in-vessel T-inventory due to deposition inside the gaps of the first wall.

2. Experiments in ASDEX Upgrade

2.1. Sample exposure in the outer midplane boundary plasma

Tungsten macro brush specimens were fabricated by Ansaldo Ricerche S.R.L. as a matrix of 2×2 W-rods with 6×6mm cross-section and 0.5mm wide gaps with a depth of 10mm. The metallic purity of the used W-material from Plansee AG was >99.97% with carbon and oxygen atomic fractions $<5\times10^{-4}$. To shield the open side faces of the W-rod assembly from plasma contact, the sample was installed inside a cylindrical graphite shield which left only the front side exposed (Figure 1). The sample was exposed to 35 plasma discharges in ASDEX Upgrade using the mid-plane manipulator system with the sample front face at a position 30cm above the midplane and 5cm inside the limiter shadow of the ICRH antenna protection limiters (Figure 2). The total exposure time in the 31 H-mode and 4 L-mode discharges was 235s. The surface temperature of the graphite shield was measured using a thermography system. Within the 4-6 seconds flat-top time of the discharges the surface temperature increased from ambient temperature (20ºC) to 150-250ºC. Since the sample was not in direct contact with the 10mm thick shield cylinder, one can conclude that the tungsten bulk temperature during the discharge stayed well below these values.

After exposure, the sample was retrieved from the machine and the W rods were cut from their base for ion beam analysis of the interior side faces. The total area densities of deuterium, carbon and oxygen were determined with Nuclear Reaction Analysis (NRA) using a 2.4MeV ^{3}He-beam and detecting the integral amount of protons from the reactions D(^{3}He,p)α, ^{12}C(^{3}He,p)^{14}N and ^{16}O(^{3}He,p)^{18}F. The D-inventories agree very well for all side faces except for the points close to the gap entrance, which show some variation, with higher values for those side faces, where the entrance edge was shadowed from the incident plasma ion flux. Figure 3a shows the average deuterium area density as a function of the distance

from the gap entrance for the gap sides with plasma exposed and shadowed entrance edge. The decrease of the D-deposition into the gap can be described by a sum of two exponentials with fall-off-lengths of 0.5-1mm and 4-13mm respectively.

In contrast to the deuterium result, the carbon area density decreases from the gap entrance towards a constant level of $\approx 10^{17}/\mathrm{cm}^2$, which is even higher for oxygen ($\approx 2-4\times10^{17}/\mathrm{cm}^2$). These values are at least by a factor of 10 above those expected from the respective concentrations in the raw W-material and result from the cutting procedure for the gaps. The deposited amount of carbon can be derived by subtraction of the constant background level, however, with increasing experimental error for the regions further away from the gap entrance where the total carbon amount gets close to the background. Figure 3b shows the resulting area density of deposited carbon as a function of the distance from the gap entrance. One obtains a D/C ratio of 0.5-0.6 at the gap entrance increasing to ≈1 deeper inside the gap. For the points near the gap bottom D/C cannot be determined because of the diverging error resulting from the carbon background subtraction. The increase of the D/C ratio away from the entrance can be qualitatively explained by a corresponding temperature gradient from the exposed front surface towards the cooler base.

Unfortunately there are no accurate local data on both the local D-ion flux and the neutral fuel recycling flux at the gap entry. Further uncertainty results from possible local carbon sources due to erosion of the graphite shield with correspondingly increased co-deposition in the probe gaps. Therefore it is not possible to derive reliable values of the D-retention fraction for the samples exposed at the midplane plasma boundary.

2.2. Sample exposure at the outer divertor target plate in ASDEX Upgrade

For measurements of D/C deposition at gap side walls in the divertor of ASDEX Upgrade, a probe head was constructed for exposure at the outer target plate using the available divertor

manipulator system. To facilitate measurements and to allow re-use of the samples, a modular probe head (Figure 4) was constructed with a matrix of 2×2 rods of high purity tungsten with 8×8mm cross-section, a gap depth of 16mm and adjustable gap width (0.5 or 1mm). The encasement of the rods was also made of tungsten. To prevent gradual temperature increase in subsequent discharges, the probe head in exposure position is attached to the target plate cooling system. The W-gap sample was exposed to 3 identical H-mode discharges ≈2cm above the strike point (Figure 2) with a total exposure time of 17s. The local flux and temperature were measured using a Langmuir probe at the same poloidal position. Average values in between ELMs were $3\times10^{18}\,\mathrm{cm^{-2}s^{-1}}$ and $T_e = 9\mathrm{eV}$ resulting in a total D^+ fluence of $5\times10^{19}\,/\,\mathrm{cm^2}$ to the sample surface. The local field line inclination to the sample surface was ≈2º. The surface temperature was measured using thermography at a graphite target plate. The combination of heat capacity and thermal conductivity of graphite and tungsten lead to very similar thermal response to the incident heat flux, so that the measured temperature values are representative for the probe. During the discharge the surface temperature increased within 6s from 30ºC to 230ºC and then on the same time scale back to ambient temperature.

After exposure the sample was retrieved and disassembled for ion beam analysis as described in section 2.1. Figure 5a shows the deuterium area density as a function of distance from the gap entrance for the poloidal gaps with plasma exposed and shadowed entrance edge respectively. The carbon area density (Figure 5b) also decreases with increasing distance from the gap entrance to a constant level of $\approx 1\times10^{17}\,/\,\mathrm{cm^2}$. This constant carbon amount is about 10 times higher than expected from the carbon concentration in the W raw material. As it extends to areas of the W rods, which were covered in the probe head assembly, it is clearly not a result of the plasma expsoure. After subtracting this background level, one obtains a D/C ratio of ≈0.5 near the gap entrance similar to the value at the sample exposed to the midplane plasma periphery. Further away from the gap entrance the D/C ratio can not be

reliably determined because of the high relative error introduced by the carbon background subtraction.

Similarly to the results obtained at the main plasma periphery (section 2.1), the decrease of the D-deposition into the gap can be described by a sum of two exponentials. For the divertor probe the fall-off-lengths are 0.6-1mm and 4-6mm respectively. By integration over the entire side surface of the W-rod one obtains the total amount of D and from that a retention fraction of $\approx 4\%$ of the D-flux entering the gap deposited on the side faces. As the D retention fraction due to co-deposition is limited by the available carbon in the incident flux, one has to compare this value to the C-fraction in the plasma. In ASDEX Upgrade the carbon concentration in the confined plasma is in the range of 1% [11]. Taking into account that the local C-fraction in the divertor plasma is higher due to the local erosion source, the measured carbon concentration is clearly compatible with the gap retention fraction of 4%.

2.3. Comparison to TEXTOR experiments

In TEXTOR a probe head with similar gap structure made of 10×10 mm molybdenum alloy (TZM) blocks with 0.5mm gap width and 10mm gap depth was exposed to the plasma boundary [9,10]. In this case the local B-field inclination angle to the surface was 20º. Two samples were exposed in two series of similar discharges, with the first sample positioned 25mm outside the last closed flux surface and the second sample positioned 15mm outside the last closed flux surface, resulting in a 10 times higher incident ion flux $(9\times10^{20}\,\mathrm{m^{-2}s^{-1}} \rightarrow 9\times10^{21}\,\mathrm{m^{-2}s^{-1}})$ and slightly higher electron temperature $(T_e : 20 \rightarrow 25\mathrm{eV})$ in the latter case. The sample surface and bulk temperatures were also higher in the exposure closer to the LCFS $(T_{\mathrm{surf}} : 700°\mathrm{C} \rightarrow 1600°\mathrm{C},\ T_{\mathrm{bulk}} : 200°\mathrm{C} \rightarrow 240°\mathrm{C})$. The hidden side faces were analyzed after disassembly of the exposed samples using NRA similarly to the ASDEX Upgrade samples. The D-fractions of the flux entering the gaps retained at the hidden side

faces were 4% for the low-flux exposure and 0.4% for the high flux exposure [9]. The value obtained for low-flux exposure is the same as that measured in the ASDEX Upgrade divertor, while the value for high-flux exposure in TEXTOR is a factor of 10 smaller despite a similar flux as in the ASDEX Upgrade divertor (section 2.2). One possible parameter to explain the differences between the two experiments is the significantly higher material temperature in TEXTOR during the high-flux exposure. The influence of this parameter was studied by a dedicated test experiment in DIII-D described in the following section.

3. Experiments in DIII-D

Analysis of samples installed for an entire experimental campaign in ASDEX Upgrade underneath the divertor dome baffle revealed that the growth rate of hydrocarbon layers at these samples decreases strongly with increasing sample temperature [12]. The processes involved in hydrocarbon deposition in gaps are likely very similar on the microscopic scale. However the ratio of hydrocarbon mean free path to the linear dimension of the respective volumes is different and this might also hold for the composition of the hydrocarbon source flux and the neutral hydrogen pressure, which affect in turn sticking probabilities and re-erosion rates. Therefore, to study the temperature dependence of hydrocarbon retention particularly in PFC gaps, a sample for the DiMES manipulator at DIII-D was constructed, with a 2×20mm gap at the sample surface and 20×20mm Si wafers as catcher plates at the side faces of the gap. The sample can be heated and kept at constant temperature during exposure. To avoid additional heating by the incident plasma, the sample was exposed to the detached outer strike point area of DIII-D in two series of Ohmic discharges. In the first series the sample was kept at 30ºC and in the following series at 200ºC. The total exposure time was 32s in each series. The incident ion flux during the discharges derived from local electron density, $n_e = 2\times10^{20}/\mathrm{m}^3$, electron and ion temperatures, $T_e = 0.6\mathrm{eV}$, $T_i = 1.0\mathrm{eV}$ and a

magnetic field inclination to the sample surface of 1.3º was $9\times10^{20}\,m^{-2}s^{-1}$, however, one has to take into account that under the detached plasma conditions there will be a high additional neutral deuterium flux into the gap. After exposure the amount of deposited D and C at the retrieved catcher plates was measured by NRA analysis at IPP Garching. The dependency of the D and C area densities from the distance to the gap entrance are shown in Figure 6 for the side face with the entrance edge facing the incident B-field. The thickness of the transparent a-C:D layer determined by Ellipsometry agrees very well with the NRA results. In the case of the exposure at 30ºC (Figure 6a), D and C are deposited with an approximately constant ratio of D/C≈0.7 and an exponential fall-off length from the gap entrance of ≈3mm. At elevated temperature (Figure 6b) D and C are still deposited with approximate constant ratio, however, in this case the D area density is by a factor of 10 smaller than at 30ºC. The results confirm the observed differences between the hydrocarbon deposition in gaps at ASDEX Upgrade and TEXTOR and agree very well with the temperature dependency of hydrocarbon deposition at remote surfaces [12]. As the sticking probability at least of CH_3^+ hydrocarbons does not vary significantly in the relevant surface temperature range [13], one can conclude that this behaviour is a result of re-erosion processes by neutral deuterium because the D ions cannot reach the recessed surfaces inside the gap volume. The erosion rate of hydrocarbon layers by neutral hydrogen increases strongly with temperature, however, and leads to a transition from net layer deposition to net erosion in low temperature laboratory plasma experiments [14].

4. Extrapolation to ITER

Based on the experimental results on the retention fraction of deuterium, one can derive estimates for the expected tritium uptake in such gaps during an ITER discharge. The total area of the hidden PFC side faces in ITER will depend on the final construction details. However, for all major armour components engineering designs have been developed and

mock-up specimens have been manufactured for thermo mechanic tests. Based on these designs one can derive an estimate of the total surface of the gap side faces. For the divertor target strike point zones the example design consists of 28×20mm sized carbon fibre composite (CFC) mono blocks with 46mm thickness stacked in vertical columns with 0.5mm poloidal gap [15]. The target plate area of 55m^2 [16] will require ≈90000 mono blocks. From the tile dimensions one obtains a hidden side face area of 330% of the plasma exposed CFC surface. For the divertor outside the strike-point zones, the baffles and the divertor dome, the example design consists of 10×10×10mm tungsten rods with 0.5mm gaps [17]. With a total tungsten area of 140m^2 [16] there are ≈ 1200000 W-rods with a hidden side face area of 360% of the plasma exposed W-PFC surface. The main chamber wall armour example design consists of 42×47mm sized beryllium tiles with 10mm thickness and 2mm spacing bonded to a cooling structure [17]. With an ITER primary wall area of 690m^2 [16] the main chamber Be armour will have ≈300000 beryllium tiles. From the tile dimensions one derives a hidden side face area of 90% of the plasma exposed surface. If one adds up all hidden side face areas of the PFC gaps, one obtains in addition to the plasma exposed vessel surface of 890m^2 a total area of 1300m^2, where conventional detritiation methods have yet to demonstrate their efficiency.

To obtain an estimate for the formation of hydrocarbon inventories at these hidden areas, one has to take into account the distribution of the carbon and fuel ion flux to the first wall. For ITER, predictive computations have been made for the plasma boundary [5], which allow to extract estimates of the spatial distribution of both the fuel and carbon flux components. Using the simulation results for a ITER H-mode discharge, the fuel ion flux to a given wall element at the main chamber and baffle regions was assumed to be equal to the radial ion flux at the closest boundary cell of the computational grid and added to the neutral charge exchange flux. In the divertor, this extrapolation was not necessary because the target plates

define the boundary of the computational area and corresponding fluxes can be extracted directly. The carbon fraction in the plasma due to target plate erosion was computed in the simulation, resulting in a C-fraction of 0.5-3% of the fuel flux to the wall. Assuming the range of measured gap retention fractions for surface temperatures >200ºC (0.4-4%), one can now integrate over the full wall area of ITER and obtains an average T-retention in the range of 0.5-5g T per 400s ITER discharge at the hidden gap side faces. While the minimum T-uptake appears compatible with ITER operation, the range extends to values where periodic T-removal from the vessel becomes an essential necessity. In addition it should be noted that the given range is based on the assumption of a first wall with T_{surf}>200ºC everywhere. If one takes into account that the temperature deeper into the PFC gaps approaches that of the cooling medium (120ºC), it is conceivable that the actual T uptake in the gaps might be even higher, with correspondingly stronger limitations for ITER operation with a carbon based divertor. However, the projections are only valid as long as the carbon fraction in the plasma is similar to that in present day machines. Suppression of the carbon source in the divertor by beryllium eroded at the main chamber [18] might significantly reduce the carbon fraction in the plasma, with correspondingly decreased tritium co-deposition. Further studies are required to explore if this process occurs also under ITER divertor conditions.

5. Conclusions

The growth rates of hydrocarbon layers at side faces of plasma facing components and the fuel retention fraction at these hidden areas were measured by exposure of samples with gap structures to plasma discharges in the ASDEX Upgrade and DIII-D tokamaks and compared to data from similar experiments in the TEXTOR tokamak. All experiments show a decrease of the D and C amount deposited at the side faces with increasing distance from the gap entrance. Typical scale lengths are in the range of 0.5-2mm close to the gap entrance and 4-6mm deeper inside the gaps.

Apart from the carbon fraction in the plasma, the main parameter for the retention of D in co-deposited layers in gaps is the temperature of the material. At temperatures above 200ºC, the retained fraction is about 10 times smaller than at room temperature. This is a promising way to locally reduce the formation of tritium inventories, however, one has to take into account, that the problem might be just transferred to other cooler locations. Using measured retention fractions for $T_{\mathrm{wall}} > 200°\mathrm{C}$ and a wall flux distribution from predictive ITER plasma simulations, one obtains a T-uptake in PFC gaps of 0.5-5g per discharge for the present design of ITER first wall armour components.

To increase the accuracy of these predictions and to improve the understanding of the underlying hydrocarbon transport processes, the measured data will be used as a base for the validation of a model of neutral hydrocarbon transport in the gap volume including re-erosion at the gap side faces [19].

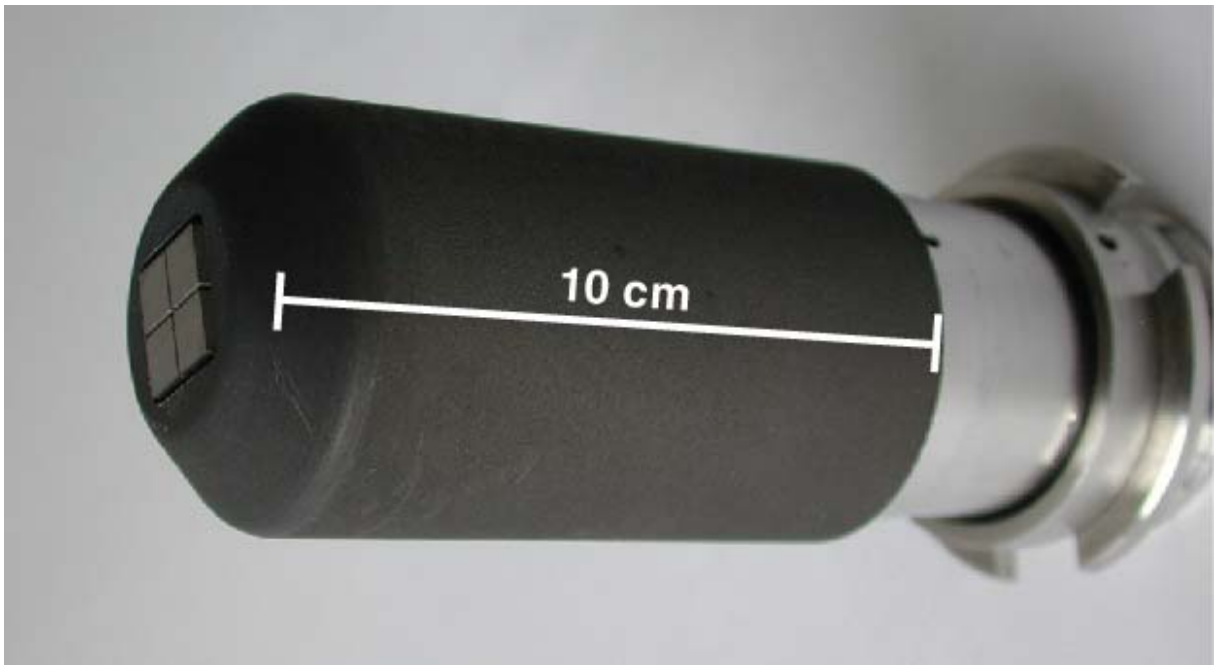

Figure 1: ASDEX Upgrade Mid-plane Manipulator probe head with installed gap sample. The graphite shield around the gap sample has an average material thickness of 1cm. The gap width between sample and shield at the front surface is ≈1mm.

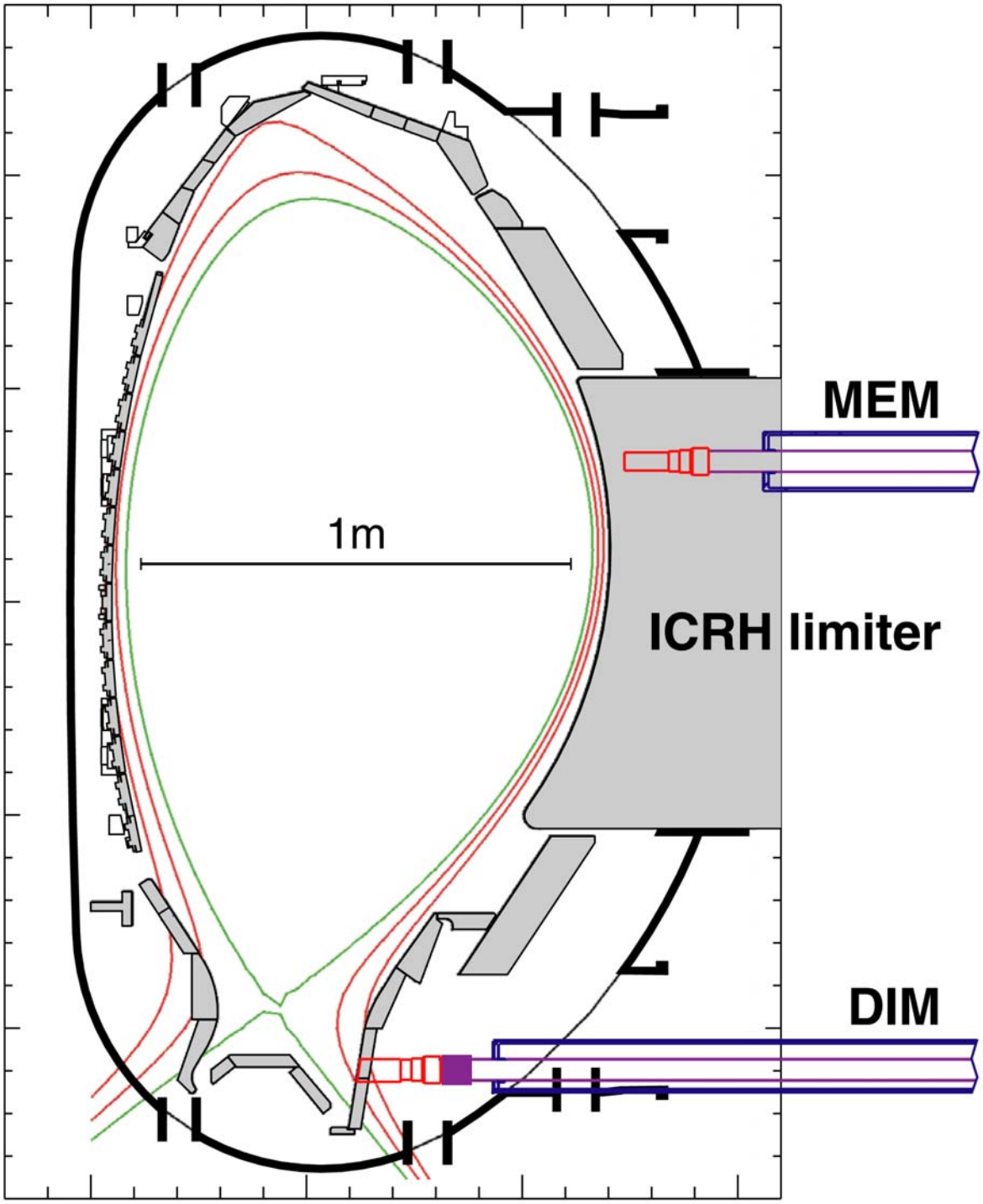

Figure 2: Cross-section of the ASDEX Upgrade vessel and plasma discharge with exposure positions of mid-plane manipulator (MEM, low field side plasma periphery) and divertor manipulator (DIM, outer divertor plate).

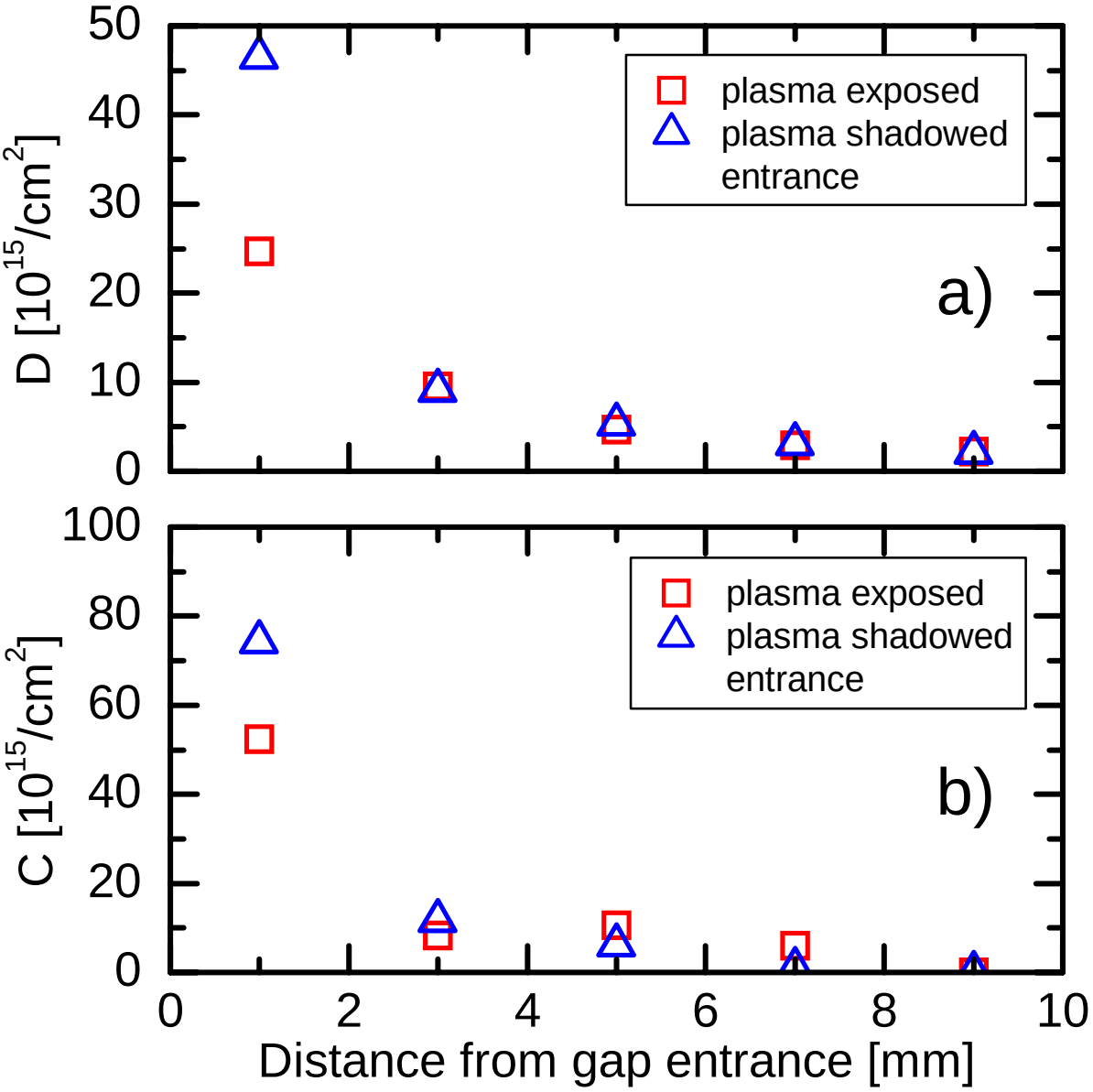

Figure 3: Area density of deuterium (a) and carbon (b) at the hidden side faces of the W-macro brush sample exposed to the ASDEX Upgrade outer plasma periphery. The data represent averages over 2 similar W-brushes. For carbon, a constant background level of $10^{17}/cm^2$ was subtracted.

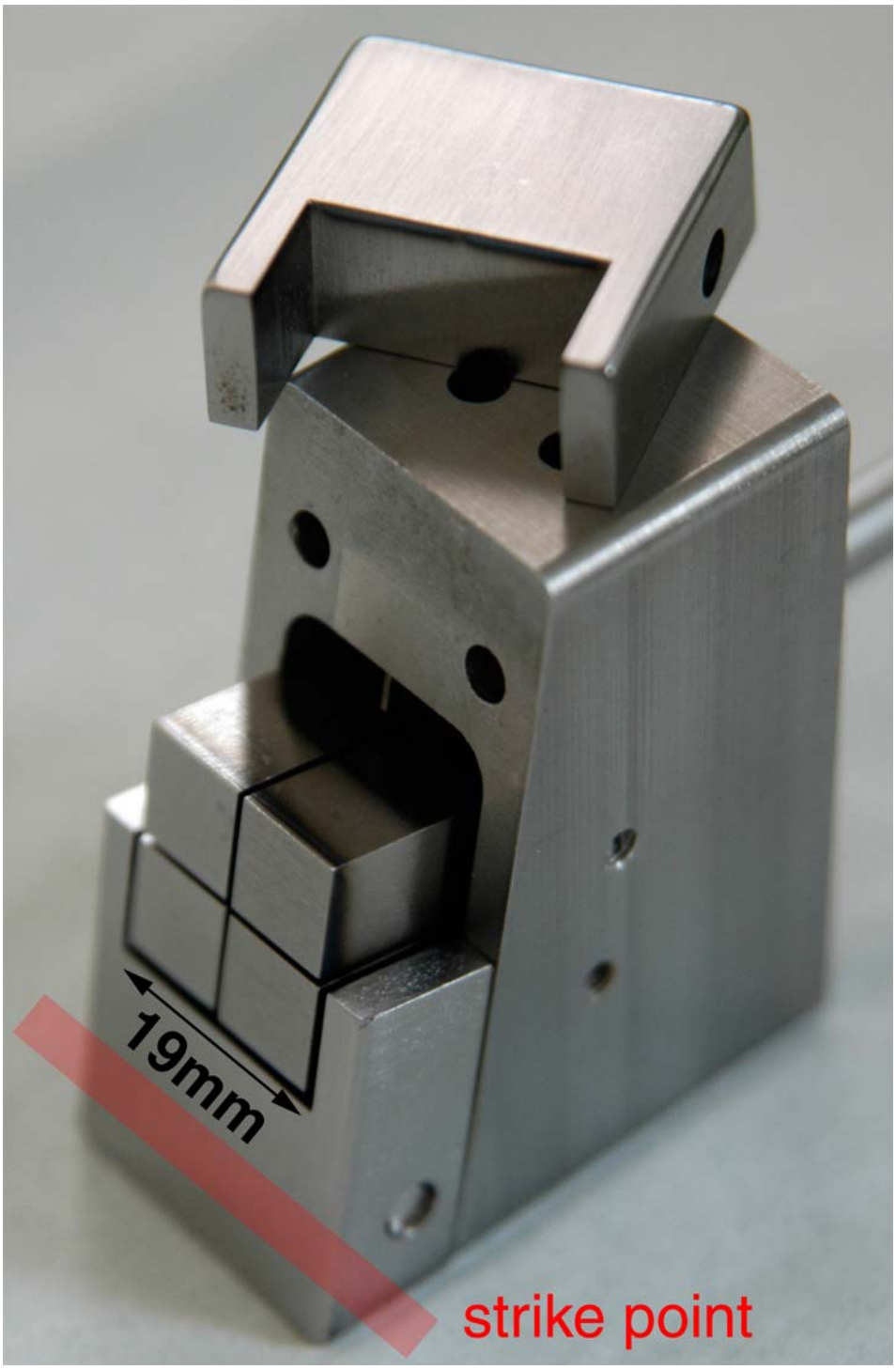

Figure 4: Partially dismantled W gap sample for the ASDEX Upgrade divertor manipulator.

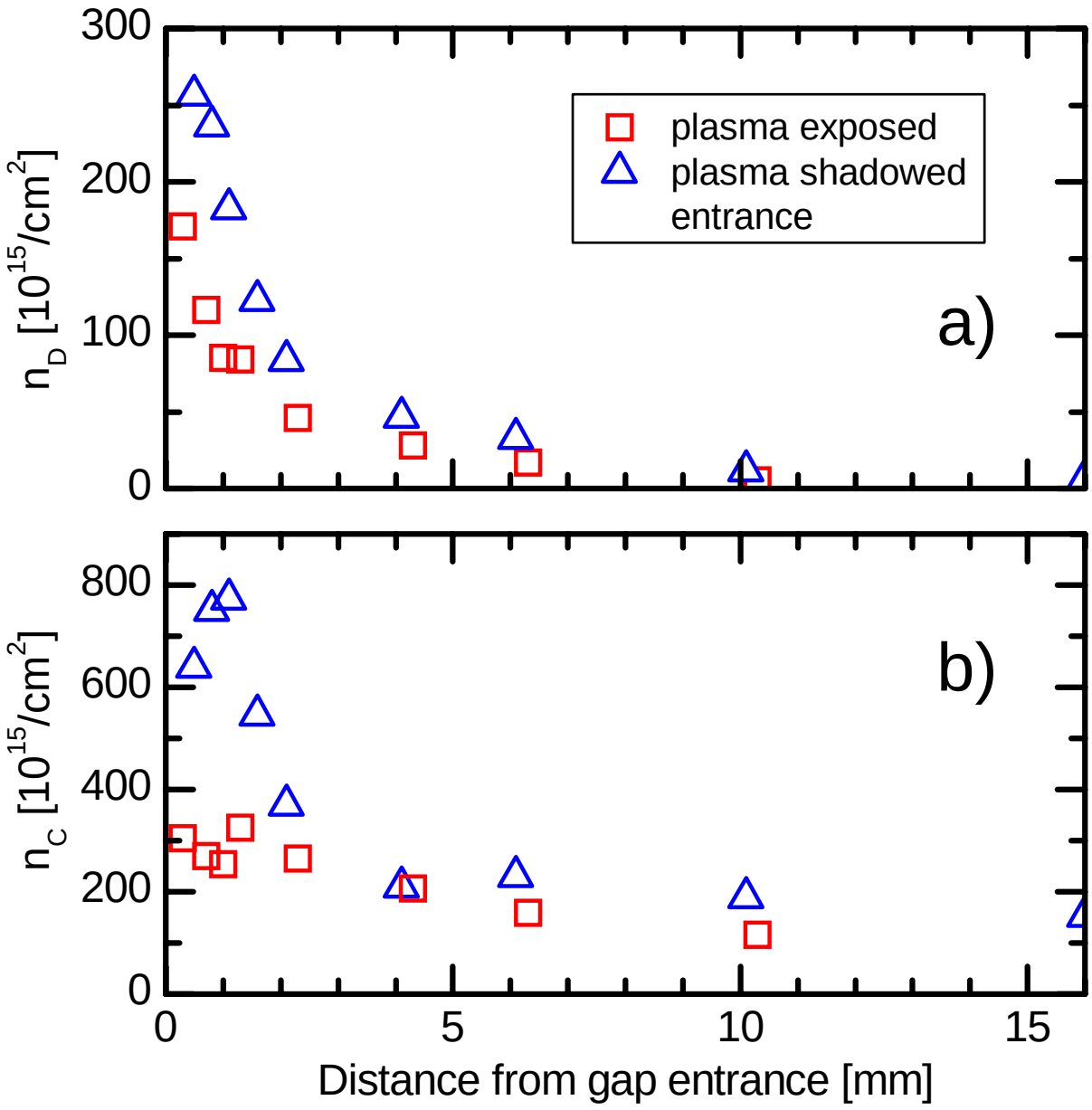

Figure 5: Area density of deuterium (a) and carbon (b) at the hidden side faces of the W-macro brush sample exposed to the ASDEX Upgrade outer strike point plasma.

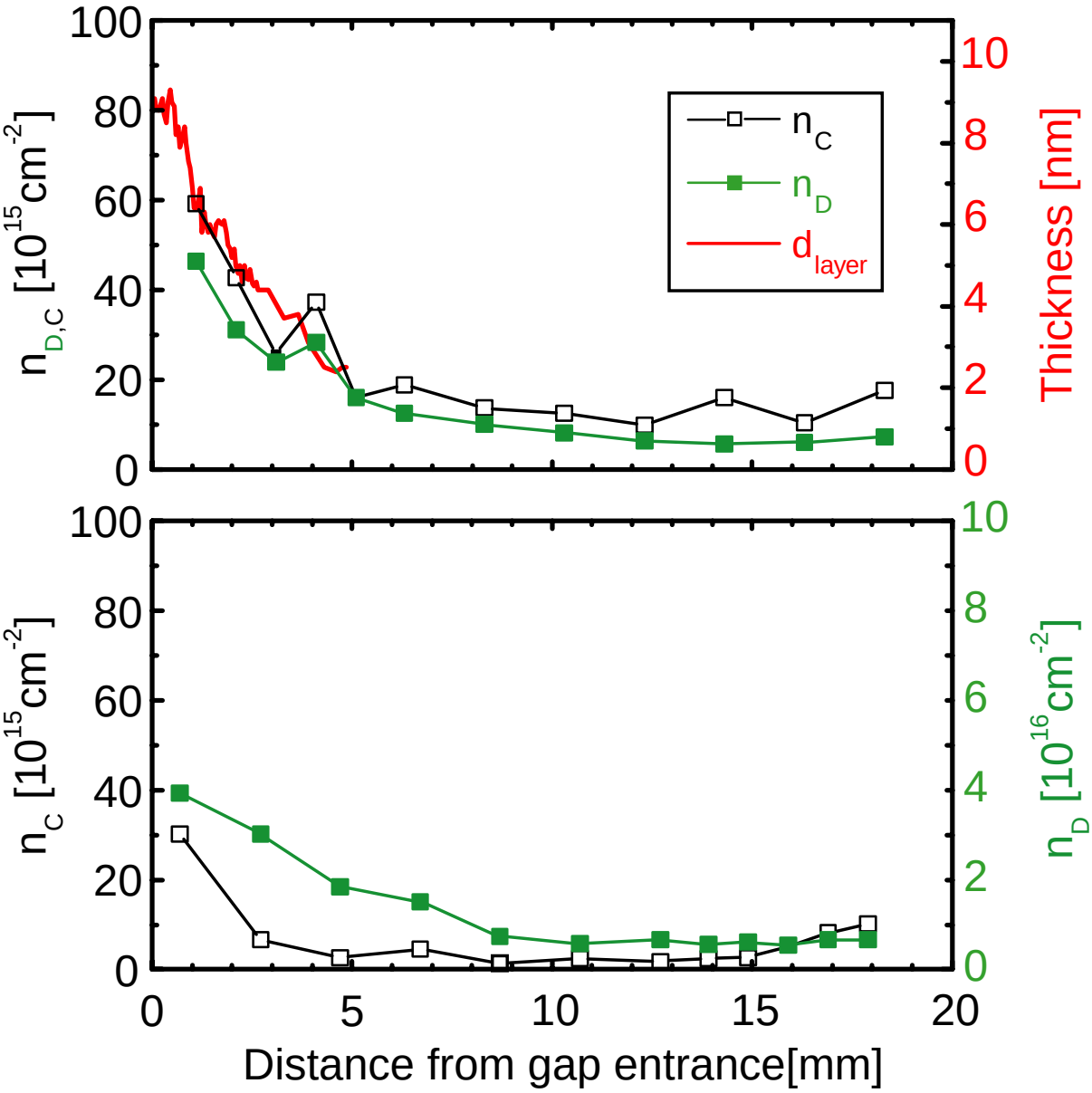

Figure 6: Area density of deuterium and carbon (b) at the hidden side faces of the DiMES gap sample exposed to a DIII-D Ohmic detached outer strike point plasma a) at ambient temperature (30ºC) and b) at 200ºC. The red line in a) represents the thickness of the a-C:D layer determined by Ellipsometry.

6. References

[1] G. Federici, J.N. Brooks, D.P. Coster, et al., Journal of Nuclear Materials **290** (2001) 260.

[2] N. Bekris, C. Caldwell-Nichols, L. Doerr, et al., Journal of Nuclear Materials **307** (2002) 1649.

[3] R.A. Causey, J.N. Brooks, G. Federici, Fusion Engineering and Design **61-2** (2002) 525.

[4] G. Federici, J.N. Brooks, M. Iseli, et al., Physica Scripta **T91** (2001) 76.

[5] A.S. Kukushkin, H.D. Pacher, G.W. Pacher, et al., Nuclear Fusion **43** (2003) 716.

[6] M. Rubel, *Overview of Co-Deposition and Fuel Inventory in Castellated DivertorStructures at JET,* ICFRM-12, Santa Barbara, 04.-09.12.2005.

[7] C. Brosset, H. Khodja, Journal of Nuclear Materials **337-339** (2005) 664.

[8] M. Mayer, V. Philipps, P. Wienhold, et al., Journal of Nuclear Materials **290** (2001) 381.

[9] A. Litnovsky, V. Philipps, A. Kirschner, et al., *Carbon transport, deposition and fuel accumulation in castellated structures exposed in TEXTOR,* ICFRM-12, Santa Barbara, 04.-09.12.2005.

[10] A. Litnovsky, V. Philipps, P. Wienhold, et al., Journal of Nuclear Materials **337-339** (2005) 917.

[11] A. Kallenbach, R. Dux, J. Harhausen, et al., 2006, *Spectroscopic investigation of carbon migration with tungsten walls in ASDEX Upgrade*, this conference.

[12] M. Mayer, V. Rohde, 2006, *Mechanism of Hydrocarbon Layer Formation below the Divertor of ASDEX Upgrade*, Nucl. Fus., in print.

[13] M. Meier, A. von Keudell, Journal of Chemical Physics **116** (2002) 5125.

[14] W. Jacob, Journal of Nuclear Materials **337-339** (2005) 839.

[15] M. Merola, G. Vieider, M. Bet, et al., Fusion Engineering and Design **56-7** (2001) 173.

[16] G. Federici, J.N. Brooks, D.P. Coster, et al., Journal of Nuclear Materials **290-293** (2001) 260.

[17] J. Linke, P. Lorenzetto, P. Majerus, et al., Fusion Science and Technology **47** (2005) 678.

[18] K. Schmid, M. Baldwin, R. Doerner, et al., Nuclear Fusion **44** (2004) 815.

[19] G. Federici, M. Mayer, G. Strohmayer, et al., Journal of Nuclear Materials **337-339** (2005) 40.

10 cm

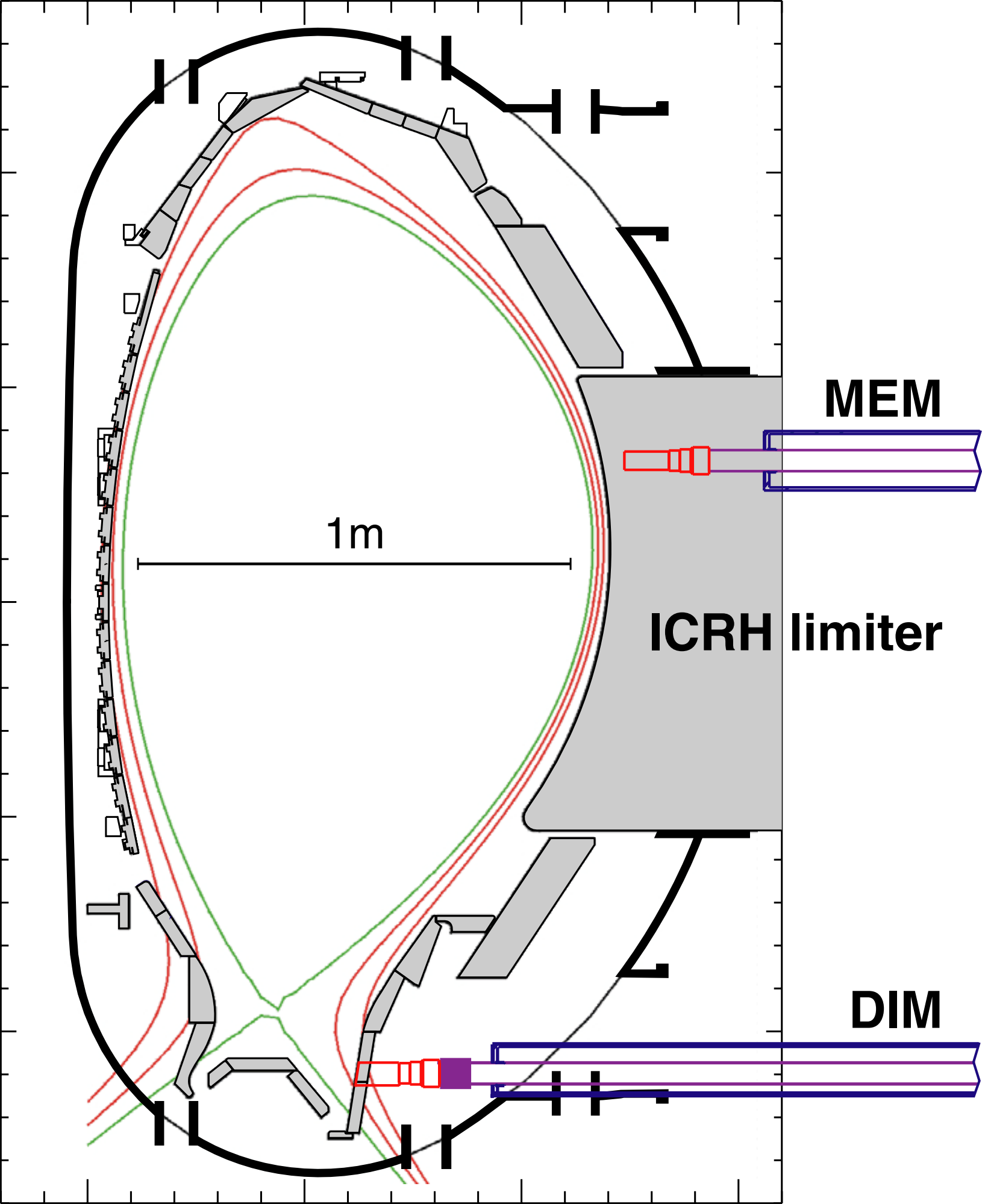
MEM
1m
ICRH limiter
DIM

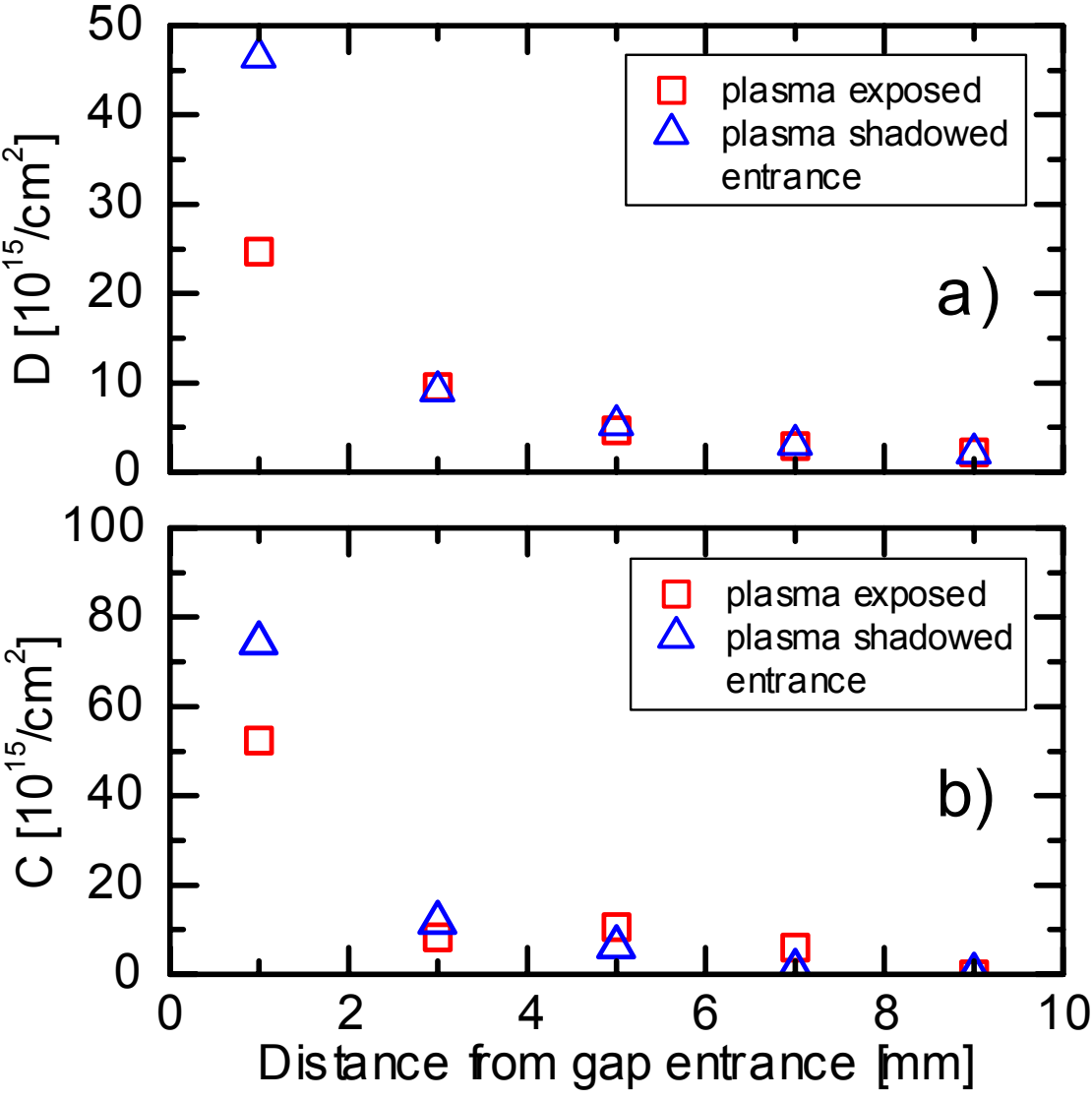
D [10^15/cm^2]
50
40
30
20
10
0
plasma exposed
plasma shadowed entrance
a)
C [10^15/cm^2]
100
80
60
40
20
0
plasma exposed
plasma shadowed entrance
b)
0
2
4
6
8
10
Distance from gap entrance [mm]

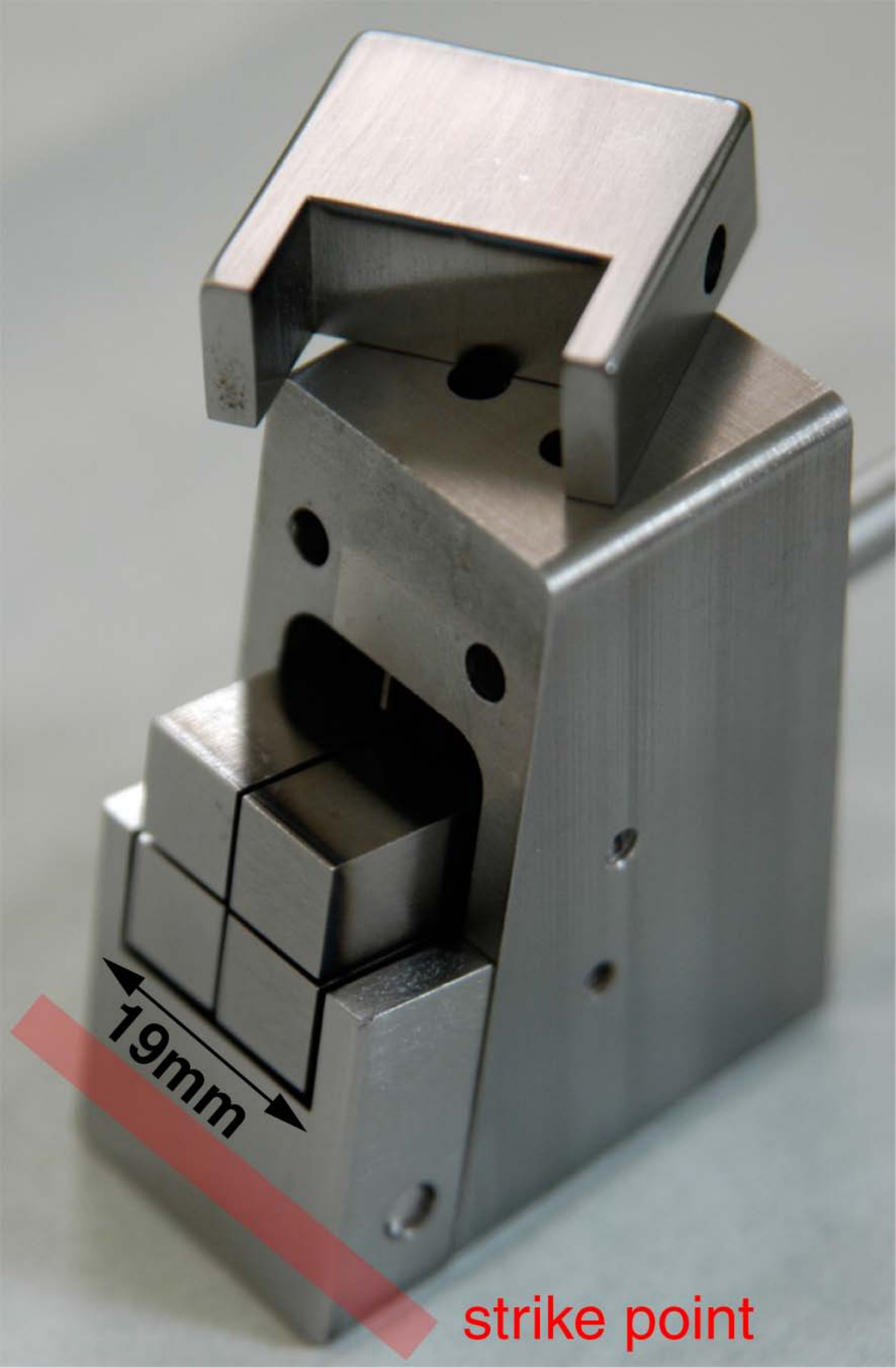
19mm
strike point

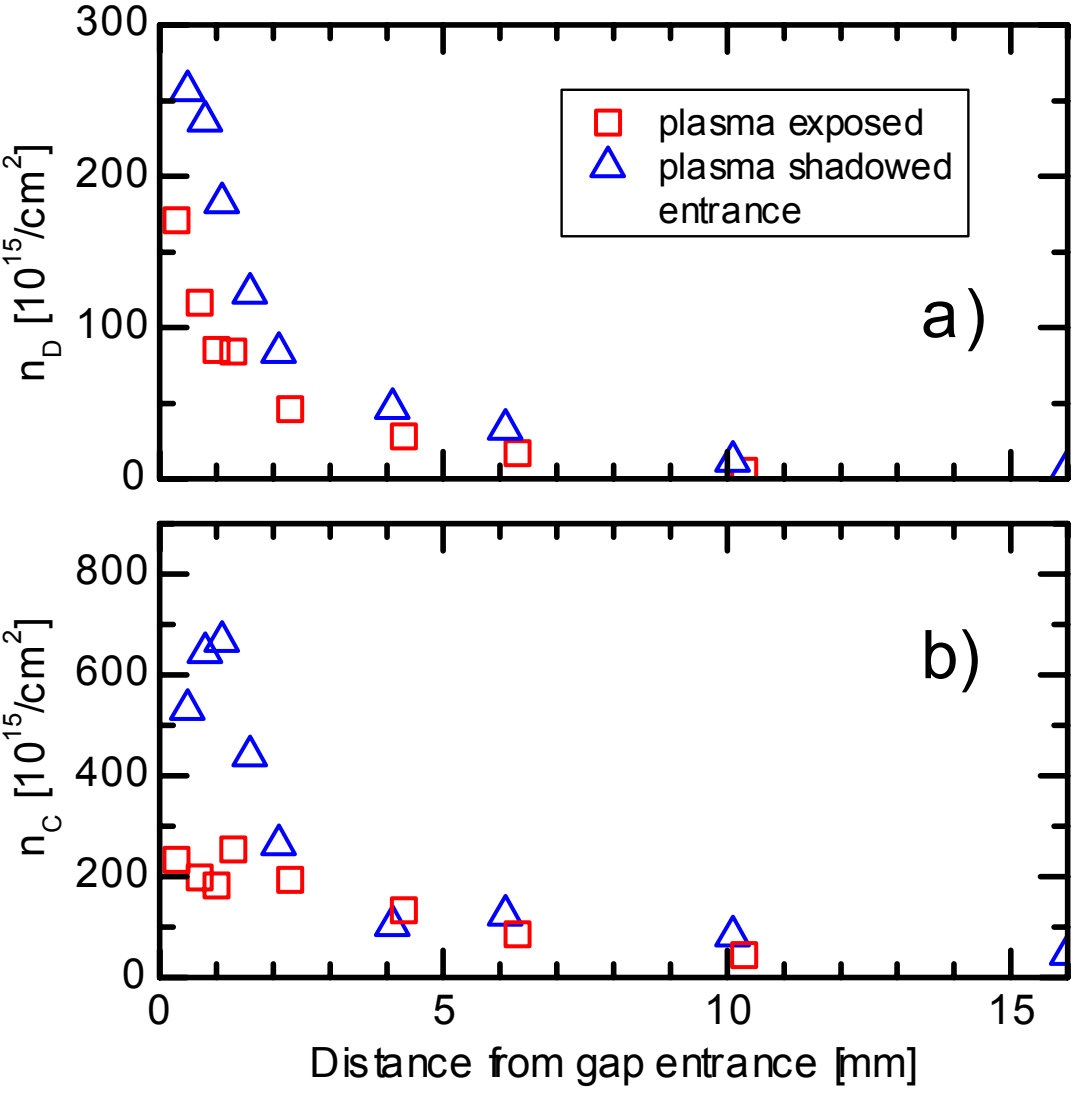
300
200
100
0
n_D [10^{15}/cm^2]
plasma exposed
plasma shadowed entrance
a)
800
600
400
200
0
n_C [10^{15}/cm^2]
b)
0
5
10
15
Distance from gap entrance [mm]

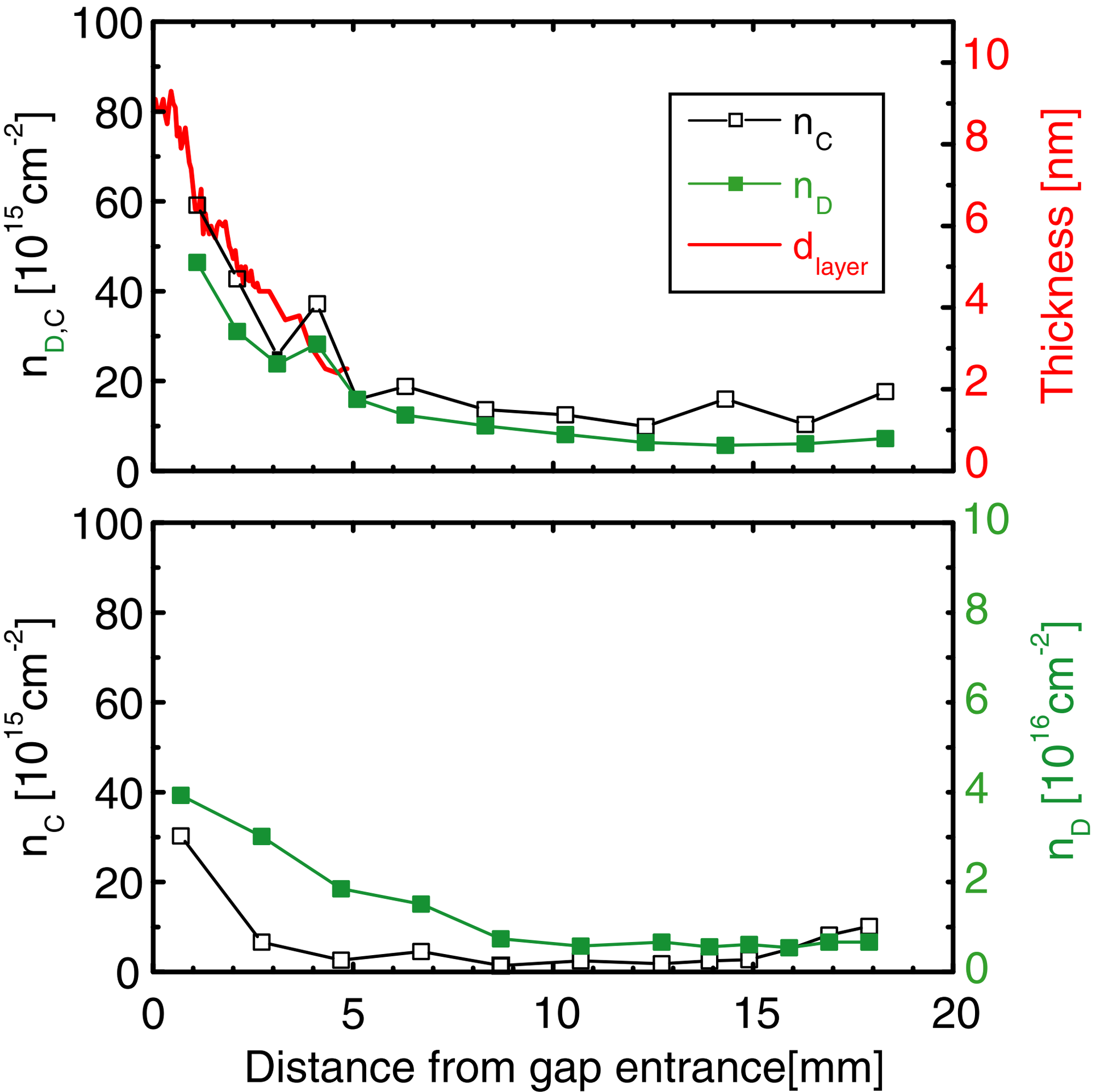
n_C
n_D
d_layer
n_D,C [10^15 cm^-2]
Thickness [nm]
n_C [10^15 cm^-2]
n_D [10^16 cm^-2]
Distance from gap entrance[mm]
0
5
10
15
20
0
20
40
60
80
100
0
2
4
6
8
10